Simultaneous observation of families and accompanied air showers at Mt. Chacaltaya. II. Study of the hadronic component in air showers

C. Aguirre,[1] H. Aoki,[2] K. Hashimoto,[3] K. Honda,[4] N. Inoue,[5] N. Kawasumi,[3] Y. Maeda,[6] N. Martinic,[1] T. Matano,[7,*] N. Ohmori,[6] A. Ohsawa,[8] K. Shinozaki,[5] M. Tamada,[9] R. Ticona,[1] and I. Tsushima[3]

[1]*Instituto de Investigaciones Fisicas, Universidad Mayor de San Andres, La Paz, Bolivia*
[2]*Faculty of Science, Soka University, Hachioji, Tokyo, 192-8577 Japan*
[3]*Faculty of Education, Yamanashi University, Kofu, 400-8510 Japan*
[4]*Faculty of Engineering, Yamanashi University, Kofu, 400-8511 Japan*
[5]*Faculty of Science, Saitama University, Urawa, 388-8570 Japan*
[6]*Faculty of Science, Kochi University, Kochi, 780-8520 Japan*
[7]*Shibakubo, Tanashi, Tokyo, 188-0014 Japan*
[8]*Institute for Cosmic Ray Research, University of Tokyo, Kashiwa, 277-8582 Japan*
[9]*Faculty of Science and Technology, Kinki University, Higashi-Osaka, 577-8502 Japan*

(Received 1 November 1999; published 6 July 2000)

An experimental setup of an air shower array, hadron calorimeter, and emulsion chamber is being carried out at Mt. Chacaltaya (5200 m, Bolivia), in order to study the hadron interaction and the primary cosmic rays in the energy region exceeding 10^{15} eV. The number of hadrons in the air shower, detected by the hadron calorimeter, is discussed mainly in this paper. A comparison with the simulation shows that the number of hadrons in the air shower is not compatible with that of the simulation, indicating that the Feynman scaling law is violated more strongly than the one assumed in the simulation at 10^{16} eV. The average mass number of the primary cosmic rays, estimated from the distribution of the number of hadrons, is $\langle \ln A \rangle = 2.8 \pm 0.5$ at 10^{16} eV.

PACS number(s): 13.85.Tp, 13.85.Hd, 96.40.De, 96.40.Pq

I. INTRODUCTION

An experimental setup of an air shower array, hadron calorimeter, and emulsion chamber is being carried out at Mt. Chacaltaya (5200 m, Bolivia). The emulsion chamber detects high-energy particles in the air shower and these are called the ''family.'' In this way the experiment simultaneously supplies data of the electron component in the air shower together with those of high-energy particles in the air shower.

Emulsion chamber experiments and air shower experiments, which have been carried out independently so far, accumulate a large amount of data, respectively. Hence it is interesting and important to bridge the data by both experiments and a large scale new experimental setup is not needed for it.

The present experiment enables us to study the structure of the air showers, the nuclear interactions and the primary cosmic rays in the energy region of 10^{15}–10^{17} eV. A detailed knowledge of air shower development is important in particular at present because there are experiments, running or as a project, which intend to discriminate air showers of γ origin from those of proton origin by their inner structure [1]. On the other hand, the energy region of 10^{15}–10^{17} eV is important both for particle physics and for astrophysics, too. It is so in particle physics because this region is not covered by the existing accelerators and because there are several reports, experimental and theoretical, which point out the change of the nuclear interaction characteristics and/or existence of exotic phenomena [2–5]. It is important also under the astrophysics viewpoint, because the primary cosmic-ray spectrum has a bend, called the knee, at $\sim 10^{15}$ eV [6,7].

In our previous article, we reported the details of the experimental procedure and discussed mainly the relation between the families and the accompanied air showers [2].

Our conclusions are the following.

(1) The family does not have a strong correlation with the accompanied air shower. That is, if one fixes the total observed energy of the family at ΣE_γ, the energy spectrum of γ rays[1] in the family is similar to one another irrespective of the size of the accompanied air shower N_e. Hence we discussed that the families of $\Sigma E_\gamma = 10 \sim 10^2$ TeV are produced near above the emulsion chamber mainly by a small number (one or two) of high-energy hadronic interactions in the air shower.

(2) The relation of ΣE_γ vs N_e in the experiment is not compatible with that by the simulation where ''normal'' composition and the UA5 algorithm are assumed for the primary cosmic rays and for nuclear interactions. (See Appendix A for the assumptions in the simulation.) That is, the experimental data indicate that energy subdivision through the propagation of cosmic rays in the atmosphere is more rapid than the one assumed in the simulation. This strong subdivision of energy cannot be attained by the hypothesis of

*Deceased.

[1]The high-energy electrons and photons are called γ rays collectively in emulsion chamber experiments, because they cannot be discriminated.

the heavy-dominant primary cosmic-ray composition, currently proposed, because most of the families are produced by protons among the primary cosmic rays. An alternative hypothesis for the strong energy subdivision is to assume that the nuclear interaction changes its characteristics in high-energy region.

(3) All the air showers are accompanied by families of $\Sigma E_{ob} \geqslant 10$ TeV in the air shower size region of $N_e > 10^7$.

In the present paper we discuss the data from the hadron calorimeter which is located beneath the emulsion chamber of 15 cm Pb thick. (See Fig. 3.) The plastic scintillator of the hadron calorimeter detects the charged particles which traverse the detector. Because a high-energy electron (or a photon), incident upon the emulsion chamber, can hardly produce electrons which arrive at the hadron calorimeter, these charged particles are produced by the hadrons, incident upon the chamber, through a nuclear cascade process in Pb of the emulsion chamber. In this way the hadron calorimeter supplies the data of the hadron component in the air shower.

The hadron component in the air shower bears more direct information on the primary cosmic-ray particle and the nuclear interaction, which initiates the air shower, than any other components, such as the electron component, the muon component, etc. It is because the hadron component is situated genetically in the upper stream of the nuclear cascade process in the atmosphere. In this sense the study of the hadronic component is important and interesting for the subjects mentioned above.

The present paper consists of five sections. In Sec. II we describe the experimental apparatus briefly and the experimental data from the hadron calorimeter. In Sec. III we show the characteristics of the hadron component in the air shower from the hadron calorimeter data. We discuss in Sec. IV the primary cosmic rays and the nuclear interactions which initiate the air shower, on the basis of the observed hadron component. That is, we estimate the average mass number $\langle \log A \rangle$ of the primary cosmic rays and discuss the characteristics of the nuclear interaction, in the energy region of 10^{16} eV. Section V is devoted to a summary and discussion.

II. EXPERIMENTAL PROCEDURE

A. Experimental apparatus

The experimental apparatus consists of the air shower array, the emulsion chamber and the hadron calorimeter (called the ''burst detector'' previously) (see Fig. 1) [2]. The air shower array consists of 35 plastic scintillators, which are distributed over a circular area of 50 m radius. The emulsion chamber and the hadron calorimeter are stored in the AS-EC room. The emulsion chamber consists of 32 units of area 50 cm $\times$ 50 cm, each of which is 15 cm Pb thick and contains 14 sensitive layers of x-ray films (and sometimes of nuclear emulsion plates for the purpose of shower energy calibration). (See Figs. 2 and 3.)

The hadron calorimeter consists of 32 units of plastic scintillator (50 cm $\times$ 50 cm $\times$ 5 cm each), which are located beneath the emulsion chamber. (See Fig. 3.) The hadron calorimeter detects a bundle of charged particles, which are produced in the emulsion chamber material by the hadron

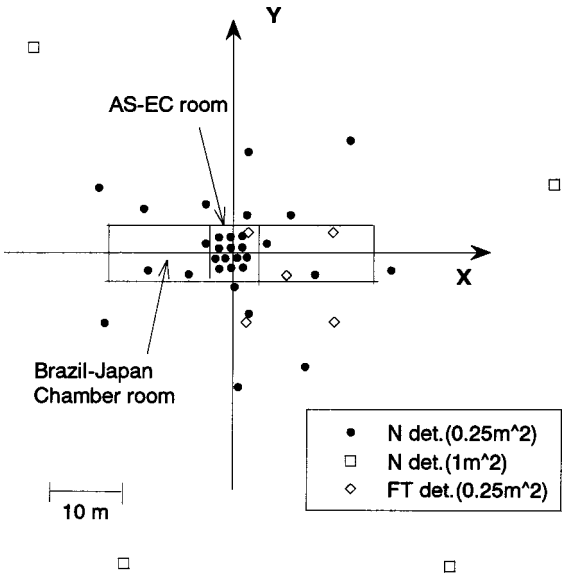

FIG. 1. Configuration of the air shower detectors. 35 scintillation detectors are distributed over an area 50 m radius from the center of the array. A room in the center of the array, indicated as the ''AS-EC room'' is for the emulsion chamber and the hadron calorimeter.

component in the air shower through local nuclear interactions. It supplies us with a clue to link the families, which have no information on the arriving time, with the air showers. That is, the family is connected to hadron component through their geometrical position and the hadron component

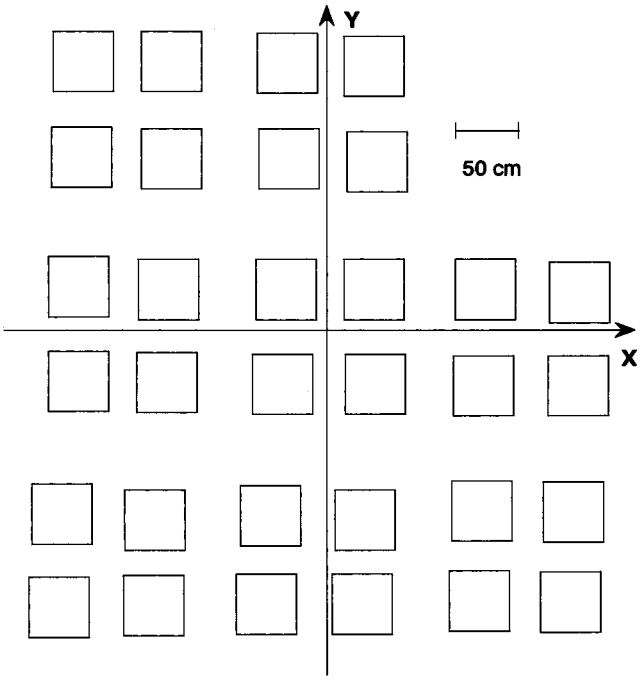

FIG. 2. Top view of the emulsion chamber. It covers 3 (m)$\times$3 (m) of area. Each unit of the chamber is 50 cm$\times$50 cm of area, and 15 cm Pb thick (equivalent to 30 c.u.). The sensitive layers of x-ray films (and nuclear emulsion plates) are inserted at every 1 cm thickness of Pb plates after 2 cm Pb from the top.

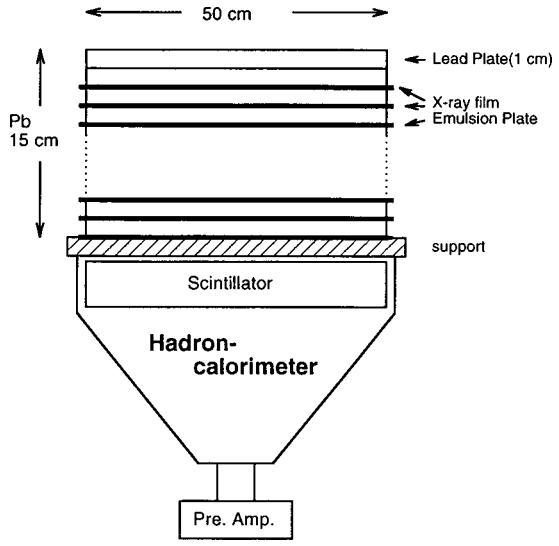

FIG. 3. Structure (the side view) of the emulsion chamber and the hadron calorimeter. One unit has the dimension of 50 cm×50 cm. The emulsion chamber unit is 15 cm Pb thick and contains 14 sensitive layers of x-ray films (and nuclear emulsion plates). The hadron calorimeter consists of a plastic scintillator 5 cm thick and a photomultiplier, which are in a box of sheet zinc.

is related to the air shower through their arriving time. (See Ref. [2] for details.)

B. Experimental data

Output from each unit of the hadron calorimeter is related to the energy deposited in the scintillator, and it is converted to a *charged* particle number using the average energy loss

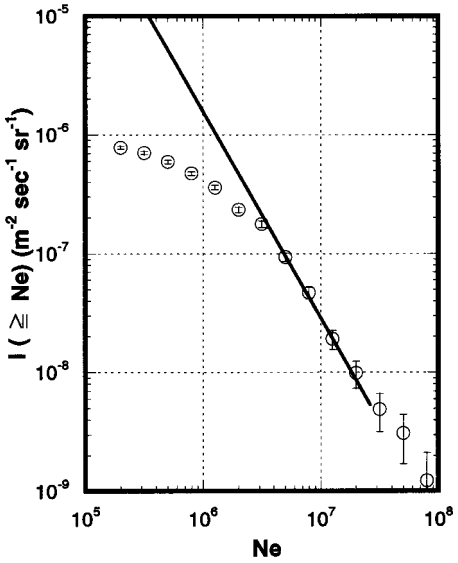

FIG. 4. Size spectra of the air showers, which are observed by two different triggering modes; the hadron-calorimeter triggering (the open circles) and the air shower triggering (the solid line). One can see that the data by the hadron-calorimeter triggering mode are biased in the size region of $N_e<5\times10^6$, compared with all the air showers one.

TABLE I. The ratio of the events (2408 events in total) where 32, $\geqslant$20, and $\geqslant$10 units among 32 of the hadron calorimeter have signals $n_b\geqslant10$ particles/0.25 m^2.

Number of units with signal	Percentage
32 units	71%
$\geqslant$ 20 units	87%
$\geqslant$ 10 units	95%

of a single muon in the scintillator. The number of charged particles per area of 50 cm $\times$ 50 cm, n_b, is called ''particle density'' hereafter. Consequently the hadron calorimeter of 32 units supplies us with the two-dimensional distribution of the particle density. Each unit of the detector is sensitive to the particle density of $n_b=10$–10^5 (particles/0.25 m^2).

The data produced by the air shower array and by the hadron calorimeter are recorded when at least one unit of the hadron calorimeter has the particle density $n_b\geqslant10^3$ (particles/0.25 m^2). In this sense the mode of the run is called ''hadron-calorimeter triggering.''

Among the recorded events those in which at least one unit of the hadron calorimeter has the particle density $n_b\geqslant10^4$ (particles/0.25 m^2) are selected for the present analysis. The number of selected events is 2408 for 4.6 years running (May 1979–November 1985), during which the emulsion chamber is active simultaneously. Figure 4 illustrates two size spectra of the air showers of the present data set and of all the air showers generated by the air shower triggering mode. The figure shows that present data set is biased by the hadron-calorimeter triggering in the air shower size region of $N_e<5\times10^6$. The average of the age parameter of the air shower in the data set is $\langle s\rangle=0.70$, which is younger compared with $\langle s\rangle=0.96$ in those of the air-shower triggering mode.

It is interesting to see how widely the hadrons are distributed in the air shower. Table I shows the fraction of events (2408 events in total) in which 32, $\geqslant$20 and $\geqslant$10 units of the hadron calorimeter have signals ($>$10 particles/0.25 m^2) among 32 units in total.

Since the density level for data selection is set high, almost all units of the hadron calorimeter have signals in the selected events. In other words, in the events which have the central particle density $n_b^{max}\geqslant10^4$ (particles/0.25 m^2), the energy flow of hadrons is larger than 10 GeV/0.25 m^2 at the distance $r=$*several* meters from the center of the air shower.[2]

C. Lateral distribution of particle density by the hadron calorimeter

1. Determination of the lateral distribution

The lateral distribution of the particle density is determined by the algorithm in Appendix B from the two-

[2]Roughly speaking, the particle density of $n_b=10$ corresponds to the hadron energy of 10 GeV on average. (See Appendix E.)

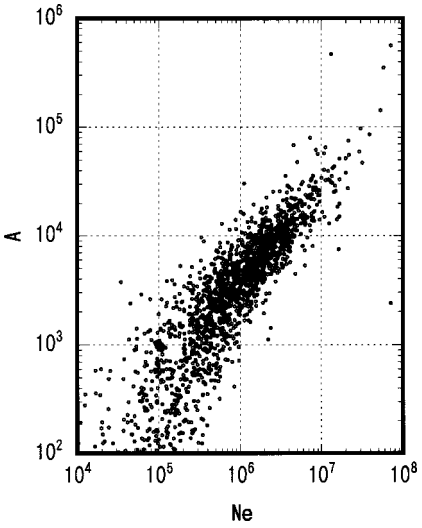

FIG. 5. The air shower size N_e and the parameter A of the lateral distribution of the particle density. [See Eq. (1) in the text.] A has a strong correlation with the air shower size.

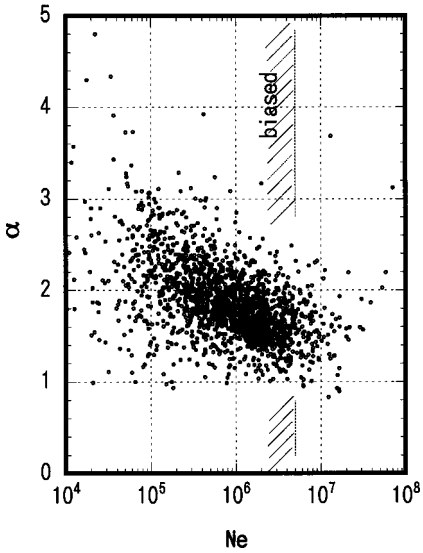

FIG. 6. The air shower size N_e and the parameter α of the lateral distribution of the particle density.

dimensional map of the particle density data. Essentially, we look for the least-squares fitting to the curve,

$$n(r)=\frac{A}{r_0^2}\left(\frac{r}{r_0}\right)^{-\alpha} \qquad (r_0=1 \ \text{m}) \tag{1}$$

moving the center of the distribution by a certain algorithm.

Thus the parameters A and α of the particle density distribution of Eq. (1) are determined for each event, together with the center of the distribution. The average distance between the center of the particle density, thus determined, and that of the air shower is 0.9 ± 0.7 (m), which shows that both agree well, taking the error of the air shower center into account. The average distance between the center of the particle density and that of the family is 0.15 ± 0.10 (m). Figures 5 and 6 present the parameters A and α in relation to the air shower size N_e, respectively, for the events which satisfy the following criteria. The criteria are for a better determination of the parameters.

(1) The center of the particle density is located inside the area which consists of the top surface of the hadron calorimeter plus the margin (50 cm wide) outside it.

(2) The air shower has an age parameter, determined by the lateral distribution of electron density, $0.2\leqslant s<1.4$.

(3) The air shower has an inclination of $\theta<50°$.

(4) The linear correlation coefficient q, which expresses the degree of the least-squares fitting of the curve Eq. (1) to the data, has a value of $-1.0\leqslant q\leqslant -0.6$. (See Appendix B.)

In these two figures one should recall that the data is biased in the region of $N_e<5\times10^6$. In the nonbiased region of $N_e>5\times10^6$, the parameters A increases almost linearly with the air shower size N_e while α looks to increase very slowly. It is a reasonable tendency because, as the primary energy or the air shower size becomes higher, the air shower becomes larger and younger at the Mt. Chacaltaya level. And correspondingly, the lateral distribution becomes steeper. The large value of α in the lower size region of $N_e<10^6$ can be attributed to the fact that the distribution must be so sharp as to fulfill the event selection condition of $n_b\geqslant10^4$ (particles/0.25 m^2). We cannot find any distinct difference of particle density distribution between the events with and without the family.[3] It shows, together with the strong correlation of A with N_e, that the hadrons, detected by the hadron calorimeter, bear the characteristics of the air shower rather than those of the family.

2. Average lateral distribution of particle density

Figure 7 shows the lateral distributions of the average particle density for several intervals of the age parameter s in the size region of $N_e=5\times10^6\sim10^7$. The average particle density is obtained by calculating the particle densities at several distances, using the parameter values of A and α for each event. [The raw data of the particle density lie in the region $r=0.5$–5 (m).] Among events with $N_e\geqslant5\times10^6$, the 83 events which satisfy the above criteria of (1)–(4) are used in the figure, in order to discuss the distribution on the most reliable data.

One sees in Fig. 7 that the younger air showers have a steeper lateral distribution of hadrons and a larger number of hadrons. These tendencies are consistent with our view of the air shower qualitatively.

Table II shows the parameters of the particle density distribution which give the best fitting to the data points.

[3]The particle density, due to the air shower, masks that due to the family. That is, a hadron with 10 TeV, typical energy of hadrons in the family, produces 10^4 charged particles in the hadron calorimeter (See Appendix E), which is comparable with those in the air shower. Therefore, if the size of the detector is smaller, e.g., not 50 cm×50 cm but 25 cm×25 cm, the difference of the particle density could be seen between the events with and without the family.

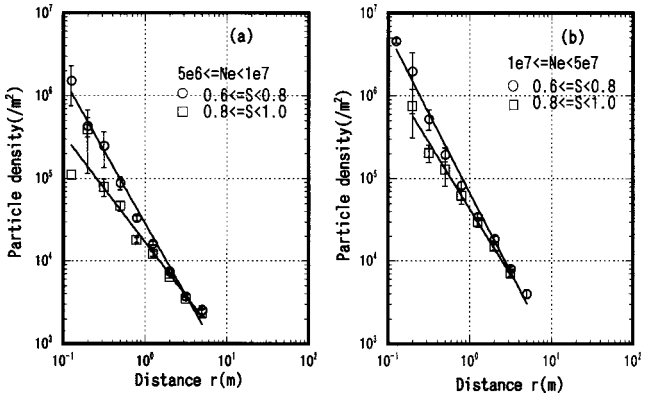

FIG. 7. Lateral distribution of the particle density, obtained by the hadron calorimeter, for the air showers of the size (a) $N_e=5\times10^6\sim10^7$ and (b) $N_e=10^7\sim5\times10^7$ and of several intervals of the age parameter. The density is the averaged one. (See the text for the averaging process.) The 72 events in the figure satisfy the criteria, mentioned in the text.

III. HADRONIC COMPONENT IN EXTENSIVE AIR SHOWERS

In the present section we estimate the energy spectrum of hadrons in the air shower from the lateral distribution of the particle density which is detected by the hadron calorimeter. We assume that all the hadrons in the air shower are charged pions.

A. Lateral distribution of the particle density by the hadrons in the air shower

Based on the electromagnetic cascade theory [8], we assume that the number of hadrons with the energy between E and $E+dE$ in the area $rdrd\phi$ at the distance r from the center is given approximately by

$$F(E,r)dE=\frac{N_0}{\pi}\left(\frac{E}{E_c}\right)^{-\gamma-1}\frac{dE}{E_c}\frac{1}{\left(\frac{K}{E}\right)^2-\left(\frac{K}{E_2}\right)^2}\theta(K-Er) \tag{2}$$

where $\theta(x)$ is the step function. The energies of hadrons E are distributed between E_1 and E_2 $(E_1<E_2)$. E_c is a constant with the dimension of energy, and K is a constant to specify the lateral distribution. (See Appendix C for the details of the above distribution.) It may be worthy to mention that we use the above formula to describe the hadron distribution in the region of our observation, i.e., 0.5 m$\leqslant r\leqslant$5 m. That is, we are not assuming that the hadrons have a fixed value of the spectral index γ over a whole range of their energies.

The constant K, which specifies the lateral spread of hadrons in the air shower as $\langle Er\rangle=(3/2)K$, depends approximately on the average value of the transverse momentum of the produced particles in multiple particle production $\langle p_T\rangle$ and 1 collision mean free path of the air at Mt. Chacaltaya $\lambda_{\rm coll}$. That is, the value of K is estimated as $K=c\langle p_T\rangle\lambda_{\rm coll}=c\times0.4$ GeV/$c\times1.6$ km$=0.64$ TeV m tentatively.[4]

Integrating the distribution with respect to r, we have the energy spectrum

$$F(E)dE=dE\int_{K/E_2}^{K/E}F(E,r)2\pi rdr=N_0\left(\frac{E}{E_c}\right)^{-\gamma-1}\frac{dE}{E_c}. \tag{3}$$

When a single pion of the energy E_0 enters the emulsion chamber of 15 cm Pb thick, the particle number, detected by the hadron calorimeter, is given by (see Appendix E)

$$N_{hc}(E_0)=\left(\frac{E_0}{E_c}\right)^{\beta}\quad(E_c=0.56\ \text{GeV},\quad\beta=1.0), \tag{4}$$

which is valid for $E_0>E_c$. Consequently, when the pions, incident upon the emulsion chamber, are distributed as $F(E,r)dE$ of Eq. (2), the particle density distribution, detected by the hadron calorimeter, is

$$n(r)=\int_{\max(E_1,E_c)}^{E_2}N_{hc}(E)\,F(E,r)dE. \tag{5}$$

It leads to (see Appendix E)

$$n(r)=\frac{N_0}{\pi(\beta-\gamma+2)}\left(\frac{E_c}{K}\right)^2\left(\frac{K}{E_cr}\right)^{\beta-\gamma+2}, \tag{6}$$

which is consistent with the empirical distribution $\propto r^{-\alpha}$. The energy spectrum $E^{-\gamma-1}dE$, assumed in Eq. (2), corresponds to the lateral distribution $1/r^{-\gamma+2}$, and therefore $1/r^{-\gamma+2+\beta}$ in Eq. (6) means the energy flow distribution of hadrons.

Comparing the above distribution with Eq. (1), we have

$$\alpha=\beta-\gamma+2, \tag{7}$$

$$A=\frac{N_0}{\pi\alpha}\left(\frac{K}{r_0E_c}\right)^{\alpha-2}. \tag{8}$$

It is worth noting that N_0 depends neither on E_1 nor on E_2 in Eq. (8). It is because the particle density at the distance r is approximately proportional to the energy flow density at r,

$$\int_{E_1}^{K/r}E^{1-\gamma+\beta}dE,$$

which depends mainly on the upper limit of the hadron energy (K/r), but weakly on the lower limit (E_1), owing to the fact of $1-\gamma+\beta>0$.

The particle density is observed in the distance of $r=0.5$–5 m by our experiment. Hence the corresponding en-

[4]A smaller value of K may be more reasonable. According to the simulation (Appendix A), the product of the energy and the lateral spread of hadrons has an average of $\langle Er\rangle=0.15$ (TeV m). The analytic calculation gives $\sqrt{\langle E^2r^2\rangle}=1.0$ (TeV m) [9]. The value is dependent on the characteristics of nuclear interaction to some extent. However, it does not change essential points of the discussion made below.

TABLE II. The parameters of the particle density distribution for the average air shower.

Air shower size N_e	Age parameter s	No. of events	Average of s $\langle s \rangle$	Lateral dist. of particles density A	α
$5\times10^6\sim10^7$	$0.4\sim0.6$	11			
	$0.6\sim0.8$	36	0.72	2.91×10^4	1.75
	$0.8\sim1.0$	13	0.85	1.71×10^4	1.30
$10^7\sim5\times10^7$	$0.6\sim0.8$	15	0.71	6.76×10^4	1.92
	$0.8\sim1.0$	8	0.86	4.31×10^4	1.61
Total		83			

ergies of hadrons range $E=0.1$–1 TeV approximately. Because in this energy region the exponent of the energy spectrum is $\gamma\simeq1.0$ according to the simulation, the lateral distribution of the particle density has the exponent $\alpha=\beta-\gamma+2\simeq2.0$, which can be seen in Fig. 6.

B. The energy spectrum of hadrons in the air shower

Figure 8 shows the averaged lateral distribution of the particle density for the air showers of $N_e=5\times10^6\sim10^7$ and $10^7\sim5\times10^7$. The averaging process is the same as in Fig. 7. The values of A, α, and N_0, obtained by assuming $K=0.64$ TeV m and $E_c=0.56$ GeV, are shown in Table III.

As mentioned above, the energy spectrum of hadrons, estimated from the lateral distribution of the particle density, is valid in the region of $E=0.1\sim1$ TeV. In other words, we cannot know the energy spectrum outside the above energy interval from the experimental data. Hence we use the differential number of hadrons at $E=1$ TeV for the purpose of the various comparisons, made below. It is given by

$$n_h\equiv\left(\frac{dN}{dE}\right)_{1\ \mathrm{TeV}}\ (\text{particles/TeV})$$
$$=N_0\left(\frac{1\ \mathrm{TeV}}{E_c}\right)^{-\gamma-1}\frac{1}{E_c}$$
$$=\pi\alpha A\left(\frac{1}{r_0}\frac{K}{1\ \mathrm{TeV}}\right)^{2-\alpha}\left(\frac{E_c}{1\ \mathrm{TeV}}\right)^{\beta}\frac{1}{1\ \mathrm{TeV}}. \qquad (9)$$

Because of $\alpha\simeq2.0$, the value of K, to be assumed, affects weakly the estimated number of hadrons in the energy region of our concern. The differential number of hadrons at $E=1$ (TeV), n_h, is presented in Table III for the air showers of $N_e=5\times10^6\sim10^7$ and $10^7\sim5\times10^7$.

Figure 9 shows the differential energy spectrum of hadrons in the air shower, given in the Table III, for the air showers of $N_e=5\times10^6\sim10^7$, together with those by the simulations. These simulations employ different models for multiple particle production; the UA5 algorithm modified for hadron-nucleus collisions (Appendix A), VENUS [10], QGSJET [11] (QCD inspired models), and HDPM [12] (semiempirical model). Atmospheric diffusion of cosmic rays is described by the code in Ref. [14] for the first one, and by CORSIKA5.20 [15] for the rest.

One can see the following in the figure.

(1) The energy spectrum of hadrons in the air shower, predicted by the simulations, agree with one another both in the number and in the power index. Detailed inspection tells us that the one using the UA5 code has a steeper power index than the others and is rather consistent with the experimental one.

(2) The energy spectrum of hadrons by the experiment is not consistent with those by the simulations in the number, while it is consistent in the power index. The number of hadrons by the experiment is smaller than those by the simulations. It is worth mentioning that, if one assumes a smaller value of K than the present one (0.64 TeV m), the discrepancy becomes larger. [See Eqs. (8) and (9).] The same tendency towards smaller hadron number is observed by the KASCADE experiment, too [16].

This is consistent with what we found in the case of high-energy γ rays in the family [2]. Therefore, both numbers of the electromagnetic and hadronic components in the air shower, which are obtained by the experiment, are less than those expected by the simulations. The implication of this discrepancy is discussed in Sec. V B.

TABLE III. The energy spectrum of hadrons in the air shower.

N_e	No. of events	A	α	γ	N_0	n_h (pcls/TeV)
$5\times10^6\sim10^7$	74	2.68×10^4	1.7	1.3	1.18×10^6	6.9×10
$10^7\sim5\times10^7$	35	5.71×10^4	1.8	1.2	1.32×10^6	1.7×10^2
(a) 8.5×10^6	8411X-02	6.9×10^4	2.5	0.5	1.6×10^4	3.8×10^2
(b) 3.0×10^7	8222X-01	1.0×10^5	1.9	1.1	1.2×10^6	3.2×10^2
(c) 5.7×10^7	0920X-90	4.0×10^5	2.3	0.7	3.5×10^5	1.8×10^3

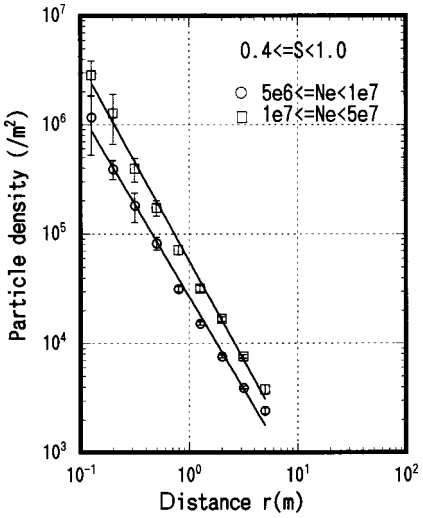

FIG. 8. Lateral distribution of particle density for the air showers of $N_e=5\times10^6\sim10^7$ and $10^7\sim5\times10^7$. The air showers are grouped by their age parameters in respective size regions. The density is the averaged one, obtained in the same way as in Fig. 7.

C. Energy spectra of hadrons by the hadron calorimeter and by the emulsion chamber

The emulsion chamber, which is located on the hadron calorimeter, detects the hadrons in the air shower, too. That is, high-energy hadrons, incident upon the chamber, make nuclear collisions with Pb in the chamber. Each collision produces a bundle of γ rays via decays of produced π^0's, and this bundle of γ rays as a whole produces a cascade shower in the chamber, which is detected by the emulsion chamber. It is interesting to compare both energy spectra of hadrons, detected by the hadron calorimeter and by the emulsion chamber.

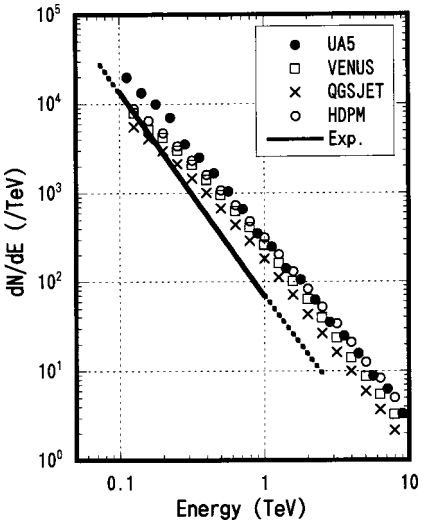

FIG. 9. Differential energy spectrum of hadrons in the air shower (the solid line) which is estimated from the lateral distribution of the particle density distribution. The size range of the air showers is $N_e=5\times10^6\sim10^7$. The predictions by various simulations are presented together. These simulations assume UA5 code (Appendix A), VENUS [10], QGSJET [11], and HDPM [12] for the nuclear collisions. The assumptions for the primary cosmic rays are the same as those in Appendix A for all the cases. The sampling of the primary energy is made for $E_0\geqslant5\times10^{15}$ eV, and the air showers with $N_e=5\times10^6\sim10^7$ are collected. The number of hadrons produced by the experiment is not compatible with the ones produced by the simulations.

If the hadrons, which have the energy spectrum of Eq. (3), enter the emulsion chamber, the differential intensity of hadron-induced showers, which are observed by the emulsion chamber, is given by

$$p\langle k^{\gamma}\rangle N_0\left(\frac{E_{ob}}{E_c}\right)^{-\gamma-1}\frac{dE_{ob}}{E_c} \tag{10}$$

where p is the probability for hadrons to make a nuclear collision in the emulsion chamber and k is the factor to convert the observed energy of a hadron-induced shower to the hadron energy, i.e., $E_{ob}=kE_h$. (See Appendix F.) Hence we can estimate the energy spectrum of hadrons, incident upon the emulsion chamber, from that which is observed by the emulsion chamber.

Figure 10 shows the differential energy spectra of hadrons in the air shower, which are observed by the emulsion chamber and by the hadron calorimeter, for three events. The selected events are those which have the number of identified hadron-induced showers exceeding 7, in order to reduce the statistical fluctuation. The characteristics of the events are shown in Tables III and IV.

It appears in Fig. 10 that there is no strong correlation between both spectra, which we found for γ rays in the family. That is, (1) We showed in the previous paper that the γ rays in the family are not correlated strongly with the size of the air shower [2]. (2) We show in the present paper that the hadrons in the family are not correlated strongly with hadrons which are estimated from the hadron calorimeter. (One should recall that the latter is correlated strongly with the size of the air shower in Fig. 5.)

IV. PRIMARY COSMIC-RAY COMPOSITION IN 10^{16} eV

We try to estimate the composition of the primary cosmic rays from the differential number of hadrons at $E=1$ TeV, n_h.

According to Ref. [17], the number of hadrons (with the energy exceeding E), which are produced by the primary proton of energy E_0, is given by

$$N_h^{(p)}(>E)=\frac{1}{2\pi i}\int\frac{d\sigma}{\sigma}\left(\frac{E_0}{E}\right)^{\sigma}f(\sigma,t),$$

where t is the atmospheric depth of the observation level.[5] The function in the integrand $f(\sigma,t)$ is dependent on the models of nuclear collisions, but is almost independent of the energy. The parameter σ is $\sigma\simeq0.8$ for hadrons at the level of Mt. Chacaltaya (5200 m) in the energy region of our concern

[5]The integration is a complex one, due to the inverse Mellin transformation.

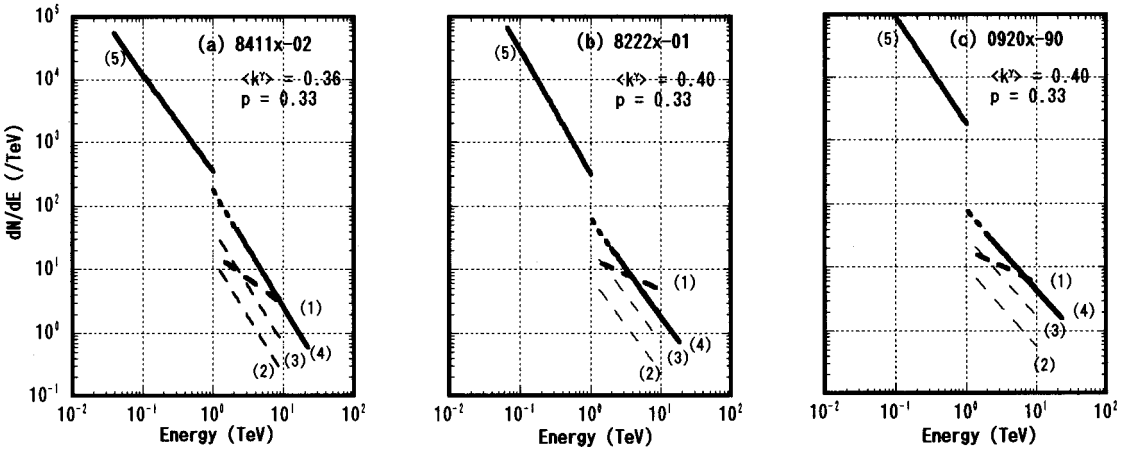

FIG. 10. Differential energy spectrum of hadrons in the air shower [the solid bold lines denoted as (4) and (5)], obtained by the emulsion chamber and by the hadron calorimeter, respectively. The numbers, attached to the lines, illustrate how to obtain the differential energy spectrum hadrons from the energy spectrum of observed hadron-induced showers in integral form (see Appendix F). Line (1): $N(>E_{ob})$ (the energy spectrum of observed hadron-induced showers in integral form), line (2): dN/dE_{ob} (the differential energy spectrum of observed hadron-induced showers), line (3): $p(dN/dE_{ob})$ (corrected for the collision probability), line (4): dN/dE [corrected for the difference between E_{ob} (the observed energy) and E (the hadron energy)]. (a), (b), and (c) of the individual events, listed in Tables IV and V, show that both spectra are not correlated strongly with each other.

[17]. The validity of the value $\sigma=0.8$ can be examined by a simulation, too. For example, the CORSIKA simulation (with QGSJET) shows that the number of hadrons (with $E>1$ TeV) is 17.5 and 100 in the air showers which are produced by the primary proton with $E_0=10^{15}$ and 10^{16} eV, respectively [18]. That is, $10^{\sigma}=10^{0.8}=6.3\simeq 100/17.5$.

If one assumes the superposition model[6] for the primary cosmic rays of atomic nucleus, we have the number of hadrons

$$N_h^{(A)}(>E)=A\frac{1}{2\pi i}\int\frac{d\sigma}{\sigma}\left(\frac{E_0/A}{E}\right)^{\sigma}f(\sigma,t)$$

for the primary cosmic ray of the energy E_0 and mass number A. Therefore, we have

TABLE IV. The events in Fig. 10.

Event	Air shower size N_e	Age parameter s	Observed energy sum[a] (TeV) γ rays	Hadrons
(a)	8.5×10^6	0.34	3.6×10^2	8.6×10
(b)	3.0×10^7	0.74	1.4×10^2	1.7×10^2
(c)	5.7×10^7	0.79	1.5×10^2	8.0×10

[a]The sum of the shower energies, observed by the emulsion chamber.

$$N_h^{(p)}(>E)\propto\frac{1}{\sigma}\left(\frac{E_0}{E}\right)^{\sigma}\quad\text{or}\quad n_h^{(p)}\equiv-\frac{dN_h^{(p)}}{dE}\propto\left(\frac{E_0}{E}\right)^{\sigma}\frac{1}{E},$$

$$N_h^{(A)}(>E)\propto\frac{A}{\sigma}\left(\frac{E_0/A}{E}\right)^{\sigma}$$

or

$$n_h^{(A)}\equiv-\frac{dN_h^{(A)}}{dE}\propto A^{1-\sigma}\left(\frac{E_0}{E}\right)^{\sigma}\frac{1}{E},$$

where n_h is the differential number of hadrons at the energy $E\,(=1\ \text{TeV})$.

Hence, we have

$$\log\frac{n_h^{(A)}}{n_h^{(p)}}=(1-\sigma)\log A,$$

which means that we can estimate $\langle\log A\rangle$ from n_h distribution.[7] That is,

$$\langle\log n_h^{(A)}\rangle-\langle\log n_h^{(p)}\rangle=(1-\sigma)\langle\log A\rangle.$$

If one can determine $\langle\log n_h^{(p)}\rangle$ only by the experiment, we can estimate $\langle\log A\rangle$ from the observed distribution of hadrons $\langle\log n_h^{(A)}\rangle$. One can see that this method of estimation is independent of the characteristics of nuclear interactions,

[6]The superposition model assumes that the primary cosmic ray of the atomic nucleus (mass number A) with the energy E_0 is described by a bundle of A nucleons with the energy E_0/A. The model is valid to describe the cosmic-ray phenomena when the observation level is deep in the atmosphere.

[7]The difference of the hadron number between the p-induced and A-induced air shower is $A^{1-\sigma}=56^{0.2}=2.2$ (for irons) by the above consideration. According to the simulation [19], if one takes into account the hadrons in the central region of the air shower, i.e., $r<0.5$ m, the difference becomes more distinct. It is because the parameter σ is smaller in the central region of the air shower.

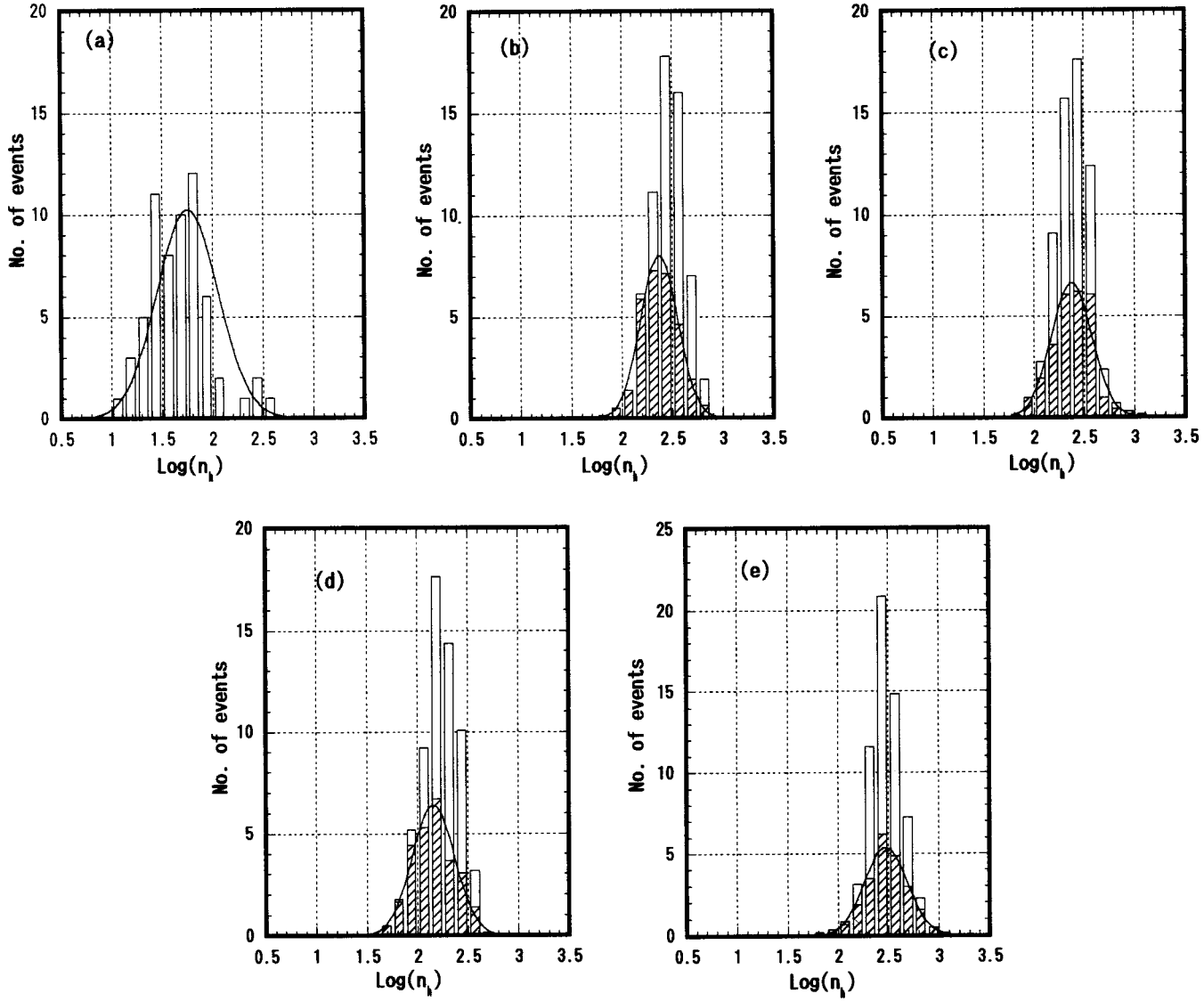

FIG. 11. Distribution of n_h (the differential number of hadrons at $E=1$ TeV). (a) The experimental data of 62 events. (b)–(e) Those by the simulations where UA5 code, VENUS, QGSJET, and HDPM are assumed for the nuclear interactions. The number of events is normalized to the experimental data. The hatched events are proton-induced ones.

which are included in the function $f(\sigma,t)$ in the equations. This point is important because the nuclear interaction models, assumed in the simulations, do not reproduce the experimental data of hadron numbers.

Figure 11(a) shows the distribution of n_h for 62 air showers which have the size of $N_e=5\times10^6\sim10^7$ with the age parameter of $s=0.2\sim1.0$. The former condition assures that the selected air showers are not biased by the hadron-calorimeter triggering, and the latter condition makes the air shower size approximately proportional to the energy of the primary particle irrespective of the characteristics of the primary particle. The air shower size of $N_e=5\times10^6$ corresponds to the primary energy of $E_0=10^{16}$ eV on average. Figures 11(b)–11(e) show the distributions of n_h by several simulations mentioned in Fig. 9.

In these figures we can see the following.

(1) The absolute value of n_h is different between those by the experiment and by the simulations, which is pointed out in the energy spectrum of hadrons in Fig. 9.

(2) The n_h distribution by the experiment is wider than that by the simulation, probably due to the experimental errors.

(3) In Figs. 11(b)–11(e) the proton-induced events occupy the left-hand side of the distribution and are distributed over eight bins in the histogram.

Using point (3) above, we assume that the $n_h^{(p)}$ distribution of the experimental data has a peak at the fourth bin from the left-hand side of the distribution. Then we have $\langle \log n_h^{(p)} \rangle = 1.44$ for the experimental data. Because the average value of the n_h distribution is 1.68 ± 0.04, we have

$$(1-\sigma)\langle \log A \rangle = 1.68-1.44=0.24.$$

Then, assuming $\sigma=0.8$, we have $\langle \log A \rangle = 1.20\pm0.22$ or

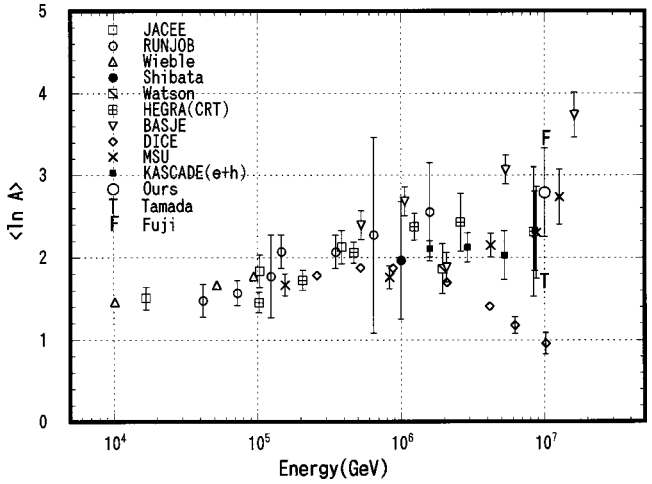

FIG. 12. Average mass number of the primary cosmic rays $\langle \ln A \rangle$, which is estimated by the number of hadrons in the air shower. The data by other experiments, compiled by the KASCADE group [20], are shown together. F and T, located at $E_0 = 10^7$ GeV, are those assumed in simulations. They are typical models of heavy-dominant [21] and proton-dominant (see Appendix A) composition, respectively.

$\langle \ln A \rangle = 2.8 \pm 0.5$. One can see that the criteria of event selection, (1)–(4) in Sec. II C, do not affect strongly the estimated value.

The value is shown in Fig. 12, together with the data by other experiments [20]. The average mass number of the primary cosmic rays looks to increase gradually with energy, but is not compatible with the one by heavy-dominant models proposed currently [21]. Astrophysical significance of the present data will be discussed elsewhere.

The present method of estimation has several advantages.

(1) The method is simple and well defined, depending only on the quantities observed by the experiment.

(2) The method does not depend on the absolute value of the hadron number n_h, but only on the shape of the distribution of n_h on log scale. One should notice that the absolute value of the hadron number depends crucially on the characteristics of the nuclear interaction, the possible change of which is pointed out in the present energy region.

(3) The method gives $\langle \ln A \rangle$, irrespective of the statistical error of n_h. The error of n_h is related to the error of the estimated value.

V. SUMMARY AND DISCUSSION

A. Nuclear interactions at 10^{16} eV

Figure 9 shows that the average number of hadrons at $E = 1$ TeV is $n_h = 6.9 \times 10$ in the size region $5 \times 10^6 < N_e < 10^7$. On the other hand, the simulations give $n_h = (1.8 \sim 3.3) \times 10^2$. It shows that the number of hadrons in the air shower is lower than that by the simulation in the energy region of 10^{16} eV. This tendency is consistent with the relationship between the families and the accompanied air showers, which is discussed in the previous paper [2]. That is, the number of γ rays in the family by the experiment is smaller than that by the simulation. It is important to point out that data of both γ rays and hadrons are independent, because they are detected by different detectors.

Therefore, the conclusions, made in the previous paper [2], are supported again by the data of hadrons in the air shower. That is, (1) The main assumptions in the simulations are on the *hadron-air* collisions and on the chemical composition of the primary cosmic rays (Appendix A). The experimental data indicate that at least either of the assumptions should be revised in the direction to make the energy subdivision more rapid. (2) Heavy-dominant hypothesis of the primary cosmic rays, proposed currently, is not effective to remove the discrepancy. (3) Hence we reach the conclusion that the nuclear interaction has different characteristics from those assumed in the simulations in the energy region of 10^{16} eV. That is, the multiple particle production in 10^{16} eV is of higher multiplicity, of softer energy spectrum of the produced particles, of larger inelasticity, etc., compared with those assumed in the simulation.

The characteristics of the nuclear interaction to describe the present data will be discussed elsewhere.

B. Average mass number of the primary cosmic-ray composition in 10^{16} eV

The average mass number of the primary cosmic rays is estimated by the number of hadrons in the air shower. The value is

$$\langle \ln A \rangle = 2.8 \pm 0.5$$

at the primary energy $\sim 10^{16}$ eV. The method of estimation is free from the characteristics of the nuclear interactions, the possible change of which is pointed out in the concerned energy region.

The value appears consistent with those by direct observation in the low-energy region of 10^{14} eV, indicating a gradual increase with the energy. However, it does not appear compatible with that by the heavy-dominant model, currently proposed.

C. Structure of air showers

An air shower consists of several components; electromagnetic (electrons and photons), hadronic, muonic, etc. Among those the electromagnetic and hadronic components of low and high energy are detected by our experimental setup, which is shown in Table V. We describe the structure of the air shower, based on the data which are obtained by the present experiment.

1. Size of the air shower

The total number of charged particles in the air shower is called the size of the air shower, which is a good measure to estimate the incident energy of the cosmic ray to initiate the air shower. (See, for example, Ref. [2].) It consists mainly of the electrons with the energies $E \geqslant 0$ [22].

TABLE V. The electromagnetic and hadronic component, observed by our experimental setup.

Component	Electromagnetic	Hadronic
High energy	(1) Emulsion chamber (2) showers/γ rays (3) $E \geqslant 1$ TeV	(1) Emulsion chamber (2) showers/hadrons (3) $E \geqslant 5$ TeV
Low energy	(1) Air shower array (2) charged/charged (3) $E \geqslant 0$	(1) Hadron calorimeter (2) charged/hadrons (3) 0.1 (TeV)$\leqslant E \leqslant 1$ (TeV)

(1) The detector (2) the detected particles/the particles concerned. (3) The energy region of the particles concerned.

2. Family in the air shower

A family consists of high-energy particles, electromagnetic and hadronic, in the air shower. At the level of Mt. Chacaltaya, most of the air showers with $N_e < 10^6$ are not accompanied by a family of $\Sigma E_{ob} > 10$ TeV, while those with $N_e > 10^7$ are always accompanied by a family. The air showers with $10^6 < N_e < 10^7$ are accompanied by the family with a certain probability. Therefore, the families in this size region have a wide fluctuation. That is a reason why the family has no strong correlation with the accompanied air showers in our experiment.

Usually we make an approximation that an air shower is originated by a single nuclear collision of the primary cosmic ray and develops by subsequent nuclear and electromagnetic cascade processes. Then, are the particles observed in the family the direct product of the same collision? If so, they would have a reasonable correlation with the characteristics of the air shower. But we found a slight correlation between the families and air showers. Hence we reach the conclusion that the family is produced by a hadron (or small number of hadrons) deep in the atmosphere. And the total observed energy is a strong constraint for the family. It is the reason why the families with the fixed value of the total observed energy have a similar energy spectrum of the constituent γ rays. The number of γ rays in the family, observed by the experiment, is smaller than that by the simulations.

3. Hadrons in the air shower

Hadrons of high and low energy are detected by the emulsion chamber and by the hadron calorimeter, respectively. (See Table V.) The low-energy hadrons have reasonable correlation with the size of the air shower, while the high-energy ones do not. The number of hadrons in the air shower, observed by the experiment, is lower than that by the simulations.

Roughly speaking, the hadrons with energy E are distributed uniformly in the circular area of $r < K/E$ ($K \simeq 0.5$ TeV m) from the center of the air shower. Hence, the hadrons which are detected by the emulsion chamber (with the energy $\geqslant 5$ TeV) and by the hadron calorimeter (with $\geqslant 0.1$ TeV) are distributed in $r < 10$ cm and $r < 5$ m, respectively. According to the simulation, the number of hadrons in the air shower is appreciably different in the region of $r < 50$ cm from the air shower center, between the air showers originated by protons and irons.

TABLE VI. Composition of the primary cosmic rays.

E_0 (eV)	Proton (%)	Alpha (%)	CNO (%)	Heavy (%)	Iron (%)	$\langle \ln A \rangle$
10^{15}	42	17	14	14	13	1.57
10^{16}	42	13	14	15	16	1.67

Note added. The energy spectra in Fig. 9, which are obtained from simulations assuming the interaction models of QGSJET, VENUS, and HDPM, show a slight bend in the low-energy region. We found that it is due to the fact that the thinning level in the simulations is set too high. If we set the level lower, the spectra are approximated by straight lines in the energy region $E = 0.1$–10 TeV. It is not necessary to revise the conclusion, extracted by Fig. 9, of a discrepancy between the experimental and the simulational data in any way.

ACKNOWLEDGMENTS

The authors wish to express their gratitude for the financial support by the Japan Society for the Promotion of Science, which made it possible to realize this international collaboration. This experiment was also supported partly by the International Scientific Research Program and Scientific Research Funds of the Ministry of Education, Science, and Culture in Japan, and by the Institute for the Cosmic Ray Research, University of Tokyo. The authors are indebted to the Bolivian staff of the Cosmic Ray Laboratory at Mt. Chacaltaya. The x-ray films and nuclear emulsions were developed at facilities of the Institute for Cosmic Ray Research, University of Tokyo.

APPENDIX A: ASSUMPTIONS IN THE SIMULATION

We describe briefly the assumptions in the simulation [2,23].

(1) *Primary cosmic rays.* The energy spectrum of the primary cosmic rays is proportional to

$$E_0^{-\gamma-1} dE_0,$$

where the index is $\gamma \simeq 1.8$ at $E_0 = 10^{15}$ eV and increases gradually to 2.0 with the energy E_0.

The composition of the primary cosmic rays is the so-called ''normal'' one, shown in Table VI.

(2) *Nuclear interactions.* The collision mean free path of hadrons in the air is

$$\lambda_{air} = 760\, \sigma_{inel}^{-0.63} \quad (\mathrm{g/cm^2}),$$

where inelastic cross section of hadrons σ_{inel} is

$$\sigma_{inel} = \sigma_0 [1 + 0.0273\epsilon + 0.01\epsilon^2 \theta(\epsilon)] \quad (\mathrm{mb})$$

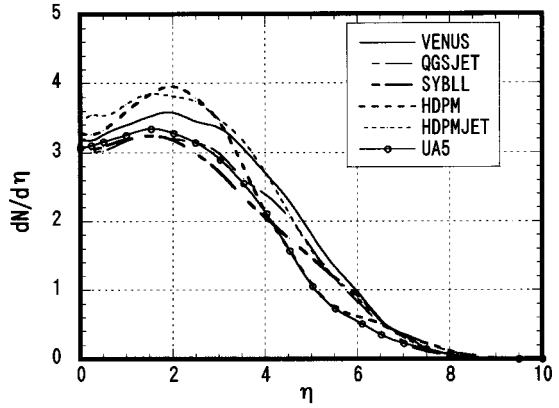

FIG. 13. The pseudorapidity distribution of produced particles at $\sqrt{s}=630$ GeV, which are predicted by several models.

with $\epsilon=\ln(E/200\ \mathrm{GeV})$. $\theta(x)$ is the step function. The constant σ_0 is 32.2 and 20.3 (mb) for the $N-N$ and $\pi-N$ collisions (N is the nucleon, π is the pion), respectively.

The collisions of the hadron in the air nucleus follows the geometrical model. That is, the number of collisions in the nucleus depends on the thickness of the nuclear matter at a given impact parameter.

In each collision of the hadron in the nucleus, the multiple particle production is described by the UA5 algorithm [24], which is a phenomenological simulation code to describe what the UA5 Collaboration observed from their experiment at CERN SPS $\overline{p}p$ collider. The pseudorapidity density of the produced particles at $\sqrt{s}=630$ GeV, predicted by UA5 code, is shown in Fig. 13 together with those by VENUS [10], QGSJET [11], HDPM [12], and SYBILL [13,15]. The figure shows that the UA5 code predicts the smallest density among the models and is consistent with them, both in the forward region and in the central region. The UA5 code predicts the energy spectrum will mildly violate the Feynman scaling law in the forward region, resulting in a slightly decreasing inelasticity of $K=0.42$ at $\sqrt{s}=546$ GeV.

(3) *Atmospheric diffusion.* The diffusion of cosmic rays in the atmosphere is by the code in Ref. [14].

APPENDIX B: ALGORITHM TO DETERMINE THE CENTER OF THE PARTICLE DENSITY DISTRIBUTION

We assume that the particle density distribution is expressed by $r^{-\alpha}$ empirically. We look for the center of the particle density distribution in the following algorithm.

(1) The center of each unit (50 cm×50 cm) of the hadron calorimeter is defined as the coordinates of the particle density.

(2) A regular square of 100 cm×100 cm, whose center is located at the center of the unit of the maximum particle density, is covered by a net of 12.5 cm×12.5 cm mesh. And each of 81 crossing points of the mesh is assumed to be the center of the particle distribution to look for the least-squares fitting. The least-squares fitting is defined as the maximum value of $|q|$, the linear correlation coefficient, mentioned below.

(3) A regular square of 25 cm×25 cm, whose center is located on the crossing point of the least-squares fitting through procedure (1), is covered by a net of 6.25 cm × 6.25 cm mesh. We look for the least-squares fitting assuming each crossing point of the mesh to be the center of the distribution.

(4) The same process is repeated for a regular square of 6.25 cm×6.25 cm which is covered by a net of 3.125 cm×3.125 cm mesh.

(5) The crossing point of the least-squares fitting through procedure (4) is defined as the center of the particle distribution.

We define the linear-correlation coefficient q as

$$q=\frac{n\sum x_i y_i-\sum x_i\cdot\sum y_i}{\sqrt{n\sum x_i^2-\sum x_i\cdot\sum x_i}\sqrt{n\sum y_i^2-\sum y_i\cdot\sum y_i}},$$

where (x_i,y_i) $(i=1,\ldots,n)$ are the data points. The linear correlation coefficient has $q=\pm1$ and $q=0$ for the complete correlation and for no correlation, respectively. In our case q is between -1 and 0.

We examine the reliability of the method using the artificially generated air showers. The distribution of the distance between the true and determined centers has the average 22.8 (cm) and the dispersion 16.2 (cm) [19].

APPENDIX C: LATERAL DISTRIBUTION OF HADRONS IN THE AIR SHOWER

According to the cascade theory of Approximation A [8], which describes the cascade process without taking the ionization loss into account and consequently is valid for electrons and photons of high energy, the number of electrons with energy between E and $E+dE$ in the infinitesimal area $dS=rdrd\phi$ at a distance r from the center is described by

$$\pi(E_0,E,r)=\frac{1}{\pi(2\pi i)^2}\int\int dsdp\left(\frac{E_0}{E}\right)^s \times\frac{1}{E}\left(\frac{E^2r^2}{K^2}\right)^{-p-1}\left(\frac{E}{K}\right)^2\Gamma(p+1)\mathcal{M}(s,p,t),$$

where K is the scattering constant and the integrals are the complex ones. If $\mathcal{M}(s,p,t)$ is a slow-varying function of p, compared with $(E^2r^2/K^2)^{-p-1}$ and $\Gamma(p+1)$, it is approximated as

$$\pi(E_0,E,r)=\frac{1}{\pi(2\pi i)}\int ds\left(\frac{E_0}{E}\right)^s\frac{1}{E}\mathcal{M}(s,\overline{p},t) \times\left(\frac{E}{K}\right)^2 e^{-E^2r^2/K^2}.$$

That is, the lateral distribution is approximated by the Gaussian distribution. To make it simpler, we approximate the Gaussian function by the step function. Consequently, we have

$$F(E,r)dE=\frac{N_0}{\pi}\left(\frac{E}{E_c}\right)^{-\gamma-1}\frac{dE}{E_c}\frac{1}{\left(\frac{K}{E}\right)^2-\left(\frac{K}{E_2}\right)^2}\theta(K-Er)$$

for the energy-lateral distribution of hadrons in the air shower. The function $\theta(x)$ is the step function. The energies of the hadrons are distributed between E_1 and E_2 ($E_1<E_2$). E_c is a constant with the dimension of the energy, and K is a constant to specify the lateral distribution.

Integrating the distribution with respect to r, we have the energy spectrum

$$F(E)dE=dE\int_{K/E_2}^{K/E}F(E,r)2\pi r dr=N_0\left(\frac{E}{E_c}\right)^{-\gamma-1}\frac{dE}{E_c}.$$

The above distribution of hadrons assumes that the hadrons of the energy E are distributed uniformly between $r=K/E_2$ ($\simeq 0$) and $r=K/E$. Or, at the distance r from the center, the energy spectrum of hadrons is $\propto E^{1-\gamma}dE$ between $E=E_1$ and $E=K/r$, and 0 in $E>K/r$.[8]

APPENDIX D: DERIVATION OF THE PARTICLE DENSITY DISTRIBUTION

From Eq. (5) in the text, we have

$$\begin{aligned}n(r)&=\int_{\max(E_1,E_c)}^{E_2}N_{hc}(E)\,F(E,r)dE\\&=\int_{\max(E_1,E_c)}^{K/r}\frac{N_0}{\pi}\left(\frac{E}{E_c}\right)^{\beta-\gamma-1}\frac{dE}{E_c}\left(\frac{E}{K}\right)^2\frac{1}{1-\left(\frac{E}{E_2}\right)^2}\\&=\int_{\max(E_1,E_c)}^{K/r}\frac{N_0}{\pi}\left(\frac{E}{E_c}\right)^{\beta-\gamma-1}\frac{dE}{E_c}\left(\frac{E}{K}\right)^2\sum_{n=0}^{\infty}\left(\frac{E}{E_2}\right)^{2n}\\&=\sum_{n=0}^{\infty}\frac{N_0}{\pi}\left(\frac{E_c}{K}\right)^2\left(\frac{E_c}{E_2}\right)^{2n}\frac{\left(\frac{K}{rE_c}\right)^{2n+\beta-\gamma+2}-\left(\frac{\max(E_1,E_c)}{E_c}\right)^{2n+\beta-\gamma+2}}{2n+\beta-\gamma+2}.\end{aligned}$$

We neglect the lateral spread of electrons in the emulsion chamber in the above calculation, because the unit size of the hadron calorimeter (50 cm×50 cm) is much larger than the lateral spread of the electron in the chamber (1 Moliére unit in Pb = 1.6 cm).

Because $K/E_c r \gg \max(E_c,E_1)/E_c$ and $2n+\beta-\gamma+2>0$, we have

$$n(r)=\frac{N_0}{\pi}\left(\frac{E_c}{K}\right)^2\left(\frac{K}{E_c r}\right)^{\beta-\gamma+2}\sum_{n=0}^{\infty}\frac{\left(\frac{K}{rE_2}\right)^{2n}}{2n+\beta-\gamma+2}.$$

Because $K/rE_2 \ll 1$, we take only the term $n=0$. That is,

$$n(r)=\frac{N_0}{\pi(\beta-\gamma+2)}\left(\frac{E_c}{K}\right)^2\left(\frac{K}{E_c r}\right)^{\beta-\gamma+2},$$

which is consistent with the empirical distribution of $\propto r^{-\alpha}$.

APPENDIX E: PARTICLE NUMBER, PRODUCED BY A HADRON

We calculate the particle number, detected by the hadron calorimeter, when a single pion of the energy E_0 hits the emulsion chamber. Strictly speaking, what is obtained by the hadron calorimeter is the total ionization loss of the charged particles in the scintillator. It is converted to the particle number through the average ionization loss in the scintillator.

Hence the particle number is related to the total track length of the charged particles in the scintillator. However, we calculate the number of charged particles (with the energy $E>0$) on the top of the hadron calorimeter instead of the total track length, because the calculation becomes simpler and because the scintillator (5 cm thick, equivalent to 0.073 collision m.f.p. or to 0.10 c.u.) is thin enough.

The hadron calorimeter is located beneath the emulsion chamber of 15 cm Pb thick. Therefore, the charged particles on the top of the hadron calorimeter (or at the bottom of the emulsion chamber) consist of the electrons and charged pions which are produced through the nuclear cascade process in Pb of the emulsion chamber.

1. Features of pion-Pb collisions

A pion of the energy E_0 collides with the Pb nucleus to cause multiple particle production. We assume that the final state of multiple particle production consists of one surviving pion and a number of produced particles. These pions have

[8]The simulated events reproduce the above spectrum approximately.

the following features. It is worth noting that most of the features, mentioned below, are established by the accelerator experiments, because the energies concerned are below 10^{13} eV.

(1) The surviving pion is one of the π^+, π^- or π^0. That is, there is a charge exchange process of the charged pion into π^0, whose probability is assumed to be $b=1/3$.

(2) All the produced particles are assumed to be pions with equal probability $c=1/3$ for three charge states, for the sake of simplicity.

(3) The energy spectrum of *charged* produced pions is expressed by

$$\varphi_0(E_0,E,K)=K\frac{2}{3}(a+1)\frac{(1-x)^a}{x}dx \quad \left(a=4.0,\ x=\frac{E}{E_0}\right),$$

which is one of the empirical formulas of the energy spectrum. Because we have

$$\int_0^{E_0} E\times\varphi(E_0,E,K)dE=\frac{2}{3}KE_0,$$

the parameter K is the total inelasticity.

(4) The total inelasticity is distributed as

$$g(K)dK=[\alpha(1-K)^{m_1-1}+\beta K^{m_2-1}]dK$$

with $\alpha=0.26$, $\beta=0.55$, $m_1=0.5$, $m_2=1.125$, leading to $\langle K\rangle=0.6$ [27].

(5) The inelastic mean free path of the pion-Pb collision is assumed to be the same as that of nucleon-Pb collision, because the size difference between pion and nucleon is affected slightly due to the large size of the target. That is,

$$\lambda=18.5 \ \text{(cm Pb)}.$$

2. Number of pions at the depth *t* in Pb

To calculate the number of pions of $E>0$, one has to take into account the energy losses of the pion through the multiple particle production and through the ionization loss. The pion loses its energy $\langle K\rangle E_0$ per collision m.f.p. through multiple particle production, and $\epsilon_\pi=\epsilon_e(\lambda/X_0)=0.24$ GeV through the ionization loss (the critical energy in Pb $\epsilon_e=7.4$ MeV and the cascade unit $X_0=0.57$ cm). Hence, when $E_0<0.4$ (GeV), the ionization loss becomes a dominant process of energy loss.

The diffusion of pions in Pb is expressed by

$$\frac{\partial F_\pi}{\partial z}=-F_\pi(E,z)+\int_0^1 g(K)dK\int_E^\infty \varphi_\pi(E',E,K)\,F_\pi(E',z)dE'+\epsilon_\pi\frac{\partial F_\pi}{\partial z},$$

where $F_\pi(E,z)dE$ is the number of pions with energy E at the depth $z=t/\lambda$. The three terms on the right-hand side of the equation correspond to the decrease of pions by collision, the increase by multiple particle production, and the decrease by ionization loss. The production spectrum of charged pions $\varphi_\pi(E_0,E,K)$ in the above equation is given by

$$\varphi_\pi(E_0,E,K)dE=[(1-b)\delta(E-(1-K)E_0)+\varphi_0(E_0,E,K)]dE,$$

where the first and the second term corresponds to the surviving pion and produced pions, respectively.

The equation has the same structure as that of the electromagnetic cascade theory under Approximation B. Hence, we have an approximate solution of

$$F_\pi(E,z)=\frac{1}{(2\pi i)^2}\int dsdq\left(\frac{E_0}{E}\right)^s\frac{1}{E}\left(\frac{\epsilon_\pi}{E}\right)^q\times\Gamma(-q)A(s,q)\,e^{\mu_\pi(s)z},$$

which is valid except for the region $z>1$. The integrations of s and q are complex ones, related to the Mellin transform. The attenuation mean free path of pions $\mu_\pi(s)$ is given by

$$\mu_\pi(s)=-1+(1-b)\langle(1-K)^s\rangle+\phi(s),$$

where

$$\langle(1-K)^s\rangle=\int_0^1(1-K)^s g(K)dK,$$

$$\phi(s)=\int_0^1 g(K)dK\int_0^1 x^s\varphi_0(E_0,E,K)dx.$$

The function $A(s,q)$ is given by

$$A(s,q)=\frac{\Gamma(s+q+1)}{\Gamma(s+1)}k(s,q),$$

where $k(s,q)$ satisfies the difference equation, corresponding to the diffusion equation, of

$$[\mu_\pi(s)-\mu_\pi(s+q)]k(s,q)=q\,k(s,q-1) \quad [k(s,0)=1].$$

This difference equation has an analytic solution of

$$k(s,q)=\Gamma(q+1)\times\frac{k(s,0)}{[h(s,0)]^q}\prod_{n=0}^{\infty}\left\{\frac{h(s,q+n)}{h(s,n)}\left(\frac{h(s,n)}{h(s,n+1)}\right)^q\right\}$$

with $h(s,q)=\mu_\pi(s)-\mu_\pi(s+q+1)$ [25].

The number of pions with the energy exceeding E is given by

$$I_\pi(E,t)=\frac{1}{(2\pi i)^2}\int\frac{dsdq}{s+q}\left(\frac{E_0}{E}\right)^s\left(\frac{\epsilon_\pi}{E}\right)^q\times\Gamma(-q)A(s,q)e^{\mu_\pi(s)z}.$$

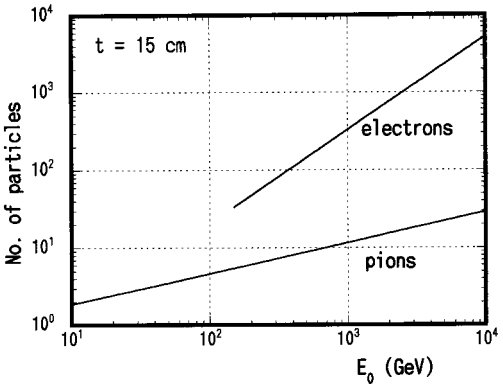

FIG. 14. Number of charged pions and electrons at the depth $t=15$ (cm Pb) in the emulsion chamber, when a pion with the energy E_0 enter the emulsion chamber.

Hence the number of pions with energy $E>0$ is given, with the help of the pole at $q=-s$, by

$$N_\pi(E_0,z)=\frac{1}{2\pi i}\int ds\left(\frac{E_0}{\epsilon_\pi}\right)^s \Gamma(s)A(s,-s)e^{\mu_\pi(s)z}.$$

The integration is evaluated by the saddle-point method, and the result is shown in Fig. 14.

3. Number of electrons

The number of π^0's of the energy E, which are produced by pion-Pb collisions at the depth t in the chamber, is given by

$$P_{\pi^0}(E,t)dEdt=\int_0^1 g(K)dK \times\int_E^\infty \varphi_{\pi^0}(E',E,K)dE\frac{dt}{\lambda}F_\pi(E',t)dE',$$

where

$$\varphi_{\pi^0}(E_0,E,K)dE=\left[b\,\delta(E-(1-K)E_0)+\frac{1}{2}\varphi_0(E_0,E,K)\right]dE.$$

The first and second terms in $\varphi_{\pi^0}(E_0,E,K)dE$ are due to the charge exchange of the surviving pion and due to the produced pions, respectively.

The production spectrum of γ rays, which are produced from π^0's through $\pi^0\to 2\gamma$ decay, is given by

$$P_\gamma(E,t)dEdt=\int_E^\infty\frac{2dE}{E'}P_{\pi^0}(E',t)dE'dt.$$

According to the cascade theory, the number of electrons at depth t with energy $E\geqslant 0$, which are produced by a single γ ray of the energy E_0 is given by

$$\Pi(E_0,0,t)=\frac{1}{2\pi i}\int\frac{ds}{s}\left(\frac{E_0}{\epsilon_e}\right)^s m(s)\,e^{\lambda_1(s)t} \times[m(s)=M(s)\sqrt{s}K_{1,0}(s,-s)].$$

Hence, the number of electrons, which are produced by these γ rays and are to be observed at depth t, is

$$\begin{aligned}N_e(E_0)&=\int_0^t\int_{E_{th}}^\infty \Pi(E',0,t-t')P_\gamma(E',t')dE'dt'\\&=\frac{1}{(2\pi i)^3}\int\frac{dsdqds'}{(s+q+1)s'(s+q-s')}\\&\quad\times\left(\frac{E_0}{E_{th}}\right)^s\left(\frac{\epsilon_\pi}{E_{th}}\right)^q\left(\frac{E_{th}}{\epsilon_e}\right)^{s'}\Gamma(-q)2\phi_{\pi^0}(s+q)\\&\quad\times A(s,q)m(s')\frac{e^{\mu_\pi(s)z}-e^{\lambda_1(s')(\lambda/X_0)z}}{\mu_\pi(s)-\lambda_1(s')(\lambda/X_0)}.\end{aligned}\tag{E1}$$

Setting $E_{th}\to 0$, we have, with the help of the pole at $s'=s+q$,

$$\begin{aligned}N_e(E_0,t)&=\frac{1}{(2\pi i)^2}\int\frac{dsdq}{(s+q+1)(s+q)}\left(\frac{E_0}{\epsilon_e}\right)^s\left(\frac{\epsilon_\pi}{\epsilon_e}\right)^q\\&\quad\times\Gamma(-q)2\phi_{\pi^0}(s+q)A(s,q)m(s+q)\\&\quad\times\frac{e^{\mu_\pi(s)z}-e^{\lambda_1(s+q)(\lambda/X_0)z}}{\mu_\pi(s)-\lambda_1(s+q)(\lambda/X_0)}.\end{aligned}$$

The integration is evaluated by the saddle point method, and the result is shown in Fig. 13.[9]

4. Particle number, detected by the hadron calorimeter

As can be seen in Fig. 13, the number of electrons is dominant to the number of pions at $t=15$ cm Pb. We approximate the relation between the number of particles, detected by the hadron calorimeter, and the energy of the pion, incident upon the emulsion chamber, as

$$N_{hc}(E_0)=\left(\frac{E_0}{E_c}\right)^\beta \quad (E_c=0.56\ \text{GeV},\ \beta=1.0).$$

The calculation by Monte Carlo method [19], made on the same assumptions, shows that

(1) The parameters in Eq. (4) in the text are

$$E_c=0.88\ \text{GeV},\quad \beta=1.01.$$

The difference may be attributed to the approximation in the numerical evaluation.

[9]When $\epsilon_\pi/E_{th}\ll 1$ and $E_{th}/\epsilon_e\ll 1$, Eq. (A1) becomes a simple formula in Ref. [26]. Both assumptions, however, do not hold simultaneously because $\epsilon_\pi=0.24$ GeV and $\epsilon_e=7.4$ MeV.

(2) The dispersion of the N_{hc} distribution is 1.44 (on $\log_{10}$ scale) at $E_0=100$ GeV, increasing with the energy.

(3) Half of the incident pions arrive at the hadron calorimeter without interactions with Pb.

APPENDIX F: ENERGY SPECTRUM OF HADRONS, OBSERVED BY THE EMULSION CHAMBER

A hadron, incident upon the emulsion chamber, makes a nuclear collision—multiple particle production—with the chamber material (Pb). The electromagnetic component, electrons and photons, among the produced particles initiate a cascade shower in the chamber, and a bundle of electrons, thus produced, in the cascade shower are detected by the sensitive layers of the emulsion chamber.

Hence we have to take two points into account for the energy spectrum of hadrons, observed by the emulsion chamber. One is that the observed energy of the hadron-induced shower is not the energy of the incident hadron but the energy of the electromagnetic component produced in multiple particle production. The other is the probability that the hadron will make nuclear collisions in the emulsion chamber.

1. Observed energy of the hadron shower

Observed energy of the hadron-induced shower E_{ob} is expressed by

$$E_{ob}=kE_h \quad (k=yK),$$

where E_h is the energy of the incident hadron. The γ-ray inelasticity k depends on the total inelasticity K and the ''*em* energy ratio'' y, both of which fluctuate widely. The total inelasticity of hadron-Pb collisions is assumed to be distributed as

$$g(K)dK=dK[\alpha(1-K)^{m_1}+\beta K^{m_2}]$$

with $\alpha=0.26$, $\beta=0.55$, $m_1=0.5$, and $m_2=1.125$, which leads to $\langle K\rangle=0.6$ [27]. The *em* energy ratio is defined as the energy ratio of the electromagnetic component to all the produced particles. It is distributed around the average value of 1/3, because almost all the produced particles are pions. Therefore, we assume the distribution to be

$$h(y)dy=\frac{1}{2c}\theta(2c-y)dy \quad \left(c=\frac{1}{3}\right).$$

Consequently the distribution of the γ-ray inelasticity is given by

$$\eta(k)dk=\int \delta(k-yK)g(K)dKh(y)dy.$$

Let the energy spectrum of hadrons, incident upon the chamber, be expressed by

$$N_0\left(\frac{E_h}{E_c}\right)^{-\gamma-1}\frac{dE_h}{E_c}.$$

Then, the energy spectrum of the hadron-induced shower is given by

$$dE_{ob}\int \delta(E_{ob}-kE_h)N_0\left(\frac{E_h}{E_c}\right)^{-\gamma-1}\frac{dE_h}{E_c}\eta(k)dk$$
$$=\langle k^\gamma\rangle N_0\left(\frac{E_{ob}}{E_c}\right)^{-\gamma-1}\frac{dE_{ob}}{E_c},$$

where

$$\langle k^\gamma\rangle\equiv\int k^\gamma\eta(k)dk=\int (yK)^\gamma g(K)dKh(y)dy$$
$$=\frac{(2c)^\gamma}{\gamma+1}[\alpha B(\gamma+1,m_1)+\beta B(\gamma+m_2,1)].$$

The inelasticity distribution is by Ref. [27].

2. Collision probability

The definition of a hadron shower is that the shower starting point is deeper than 3 cm Pb in the chamber. The showers which have a starting point deeper than 13 cm Pb are missed due to the insufficient development of the shower. Consequently, the collision probability p is given by

$$p=e^{-3.0/\lambda}-e^{-13.0/\lambda}=0.33,$$

where $\lambda=18.5$ (cm) is the collision mean free path of hadron-Pb collisions.

[1] Design Report of the Pierre Auger Project, Fermilab, 1995; P. M. Mantsch, *Proceedings of the International Symposium on Extremely High Energy Cosmic Ray Astrophysics and Future Observation*, 1996, p. 213; N. Hayashida *et al.* (Telescope Array Collaboration), *ibid.*, p. 205.

[2] N. Kawasumi, I. Tsushima, K. Honda, K. Hashimoto, T. Matano, N. Inoue, K. Mori, A. Ohsawa, M. Tamada, N. Ohmori, N. Martinic, R. Ticona, N. Gironda, F. Osco, and C. Aguirre, Phys. Rev. D **53**, 3534 (1996).

[3] C. M. G. Lattes, Y. Fujimoto, and S. Hasegawa, Phys. Rep. **65**, 151 (1980).

[4] J. D. Bjorken, Int. J. Mod. Phys. A **7**, 4189 (1992).

[5] FELIX Collaboration, E. Lippmaa *et al.*, CERN/LHCC 97-45, LHCC/I10 (1997).

[6] B. Peters, Nuovo Cimento Suppl. **14**, 436 (1959).

[7] M. Nagano, T. Hara, Y. Hatano, N. Hayashida, S. Kawaguchi, K. Kamata, T. Kifune, and Y. Mizumoto, J. Phys. G **10**, 1295 (1984).

[8] J. Nishimura, *Handbuch der Physik* (Springer, Berlin, 1967), Vol. 46/2, p. 1.

[9] A. Ohsawa and S. Yamashita, Prog. Theor. Phys. **77**, 1411 (1987).

[10] K. Werner, Phys. Rep. **232**, 87 (1993).

[11] N. N. Kalmykov and S. S. Ostapchenko, Yad. Fiz. **56**, 105 (1993) [Phys. At. Nucl. **56**, 346 (1993)]; N. N. Kalmykov, S. S. Ostapchenko, and A. I. Pavlov, Russ. Acad. Sci. Bull. Phys.

58, 1966 (1994).
[12] J. N. Capdevielle, J. Phys. G **15**, 909 (1989).
[13] R. S. Fletcher, T. K. Gaisser, P. Lipari, and T. Stanev, Phys. Rev. D **50**, 5710 (1994); J. Engel, T. K. Gaisser, P. Lipari, and T. Stanev, *ibid.* **46**, 5013 (1992).
[14] Y. Niihori, T. Shibata, I. M. Martin, E. H. Shibuya, and A. Turtelli, Jr., Phys. Rev. D **36**, 783 (1987).
[15] D. Heck, J. Knapp, J. N. Capdevielle, G. Schatz, and T. Thow, FZKA report 6019, Fortshungszentrum, Karlsruhe, GmbH Karlsruhe (1998); J. Knapp, D. Heck, and G. Schatz, Report of Forschunkszentrum, Karlsruhe, FZKA 5828 (1996).
[16] J. R. Hörandel *et al.*, Proceedings of the 26th International Cosmic Ray Conference, Vol. 1, 1999, p. 131.
[17] A. Ohsawa, Suppl. Prog. Theor. Phys. **47**, 180 (1971); T. K. Gaisser, *Cosmic Rays and Particle Physics* (Cambridge University Press, Cambridge, England, 1990).
[18] K. Shinozaki, Master thesis, Saitama University, 1999.
[19] Y. Maeda, Master thesis, Kochi University, 1999.
[20] Engler *et al.* (Ref. [16]), p. 349.
[21] M. Amenomori, E. Konishi, H. Nanjo, K. Kasahara, S. Torii, T. Yuda, T. Shirai, N. Tateyama, T. Taira, I. Mito, M. Shibata, H. Sugimoto, K. Taira, and N. Hotta, Phys. Rev. D **25**, 2807 (1982).
[22] M. Nagano, D. Heck, K. Shinozaki, N. Inoue, and J. Knapp, Report of Forschungszentrum, Karlsruhe FZKA 6191 (1998).
[23] M. Tamada, J. Phys. G **20**, 487 (1994).
[24] UA5 Collaboration, G. L. Alner *et al.*, Nucl. Phys. **B291**, 445 (1987).
[25] H. S. Snyder, Phys. Rev. **76**, 1563 (1949).
[26] C. Aguirre, H. Aoki, K. Hashimoto, K. Honda, N. Inoue, N. Kawasumi, Y. Maeda, N. Martinic, T. Matano, N. Ohmori, A. Ohsawa, K. Shinozaki, M. Tamada, R. Ticona, I. Tsushima, and K. Yokoi, Nucl. Phys. B (Proc. Suppl.) **75A**, 186 (1999).
[27] C. R. A. Augusto, S. L. C. Barroso, Y. Fujimoto, V. Kopenkin, M. Moriya, C. E. Navia, A. Ohsawa, E. H. Shibuya, and M. Tamada, Phys. Rev. D **61**, 012003 (2000).